The search for YSOs from ISOGAL data. Application to the l = +45 field

M. Felli, G. Comoretto, L. Testi, A. Omont, F. Schuller

▶ **To cite this version:**

M. Felli, G. Comoretto, L. Testi, A. Omont, F. Schuller. The search for YSOs from ISOGAL data. Application to the l = +45 field. Astronomy and Astrophysics - A&A, 2000, 362, pp.199-214. hal-04110315

HAL Id: hal-04110315
https://hal.science/hal-04110315

Submitted on 6 Jun 2023

HAL is a multi-disciplinary open access archive for the deposit and dissemination of scientific research documents, whether they are published or not. The documents may come from teaching and research institutions in France or abroad, or from public or private research centers.

L'archive ouverte pluridisciplinaire **HAL**, est destinée au dépôt et à la diffusion de documents scientifiques de niveau recherche, publiés ou non, émanant des établissements d'enseignement et de recherche français ou étrangers, des laboratoires publics ou privés.

Astron. Astrophys. 362, 199–214 (2000)

ASTRONOMY AND ASTROPHYSICS

The search for YSOs from ISOGAL data⋆,⋆⋆,⋆⋆⋆

Application to the l = +45 field

M. Felli[1], **G. Comoretto**[1], **L. Testi**[1], **A. Omont**[2], **and F. Schuller**[2]

[1] Osservatorio Astrofisico di Arcetri, Largo E. Fermi 5, 50125 Firenze, Italy
[2] Institut d'Astrophysique de Paris, CNRS, 98 bis Bd Arago, 75014 Paris, France

Received 29 February 2000 / Accepted 9 May 2000

Abstract. The 7 and 15 μm observations of the Galaxy obtained by the ISOGAL program offer an unique possibility to investigate and separate the different populations of stars in the Galactic Plane, in particular to study the population of low flux density YSOs which could not be detected with IRAS.

Considering the results obtained by ISOCAM in nearby star forming regions and in other test fields in the Galactic Plane, as well as theoretical indications, we establish criteria of general validity that can be used to select YSOs from the much larger population of Post Main Sequence (Post-MS) stars present in the ISOGAL fields. The selection is based primarily on the position of the sources in the [15] - [7]-[15] diagram, which involves only ISOGAL data and allows to select objects with IR excess as possible YSOs using the survey data alone.

The criteria are applied to five ISOGAL fields centered at l $\sim$ +45° and b $\sim$ 0°, covering a total area of 0.504 deg^2. The total number of point sources detected in both filters above the confidence limits of [7] $<$ 9.5 and [15] $<$ 8 are 386. The ISOGAL results are compared with radio observations in order to identify high luminosity YSOs out of the larger population of lower luminosity ones. We find 3 high luminosity YSOs plus 3 diffuse sources which are associated with HII regions and 35 lower luminosity YSOs. For low flux densities we find a consistent number of sources (73) detected only at 15 μm which, according to the colour upper limit, are classified as candidate YSOs.

The validity of the adopted criteria for selecting possible YSOs in the ISOGAL fields are also supported by two independent results: 1) the sources classified as YSOs and the candidate YSOs are often associated with diffuse nebulosities visible at 15 μm, landmarks of recent star forming activity, and 2) the numbers of high luminosity and low luminosity YSOs that we have found compare well with the expectations.

Key words: stars: formation – ISM: H II regions – Galaxy: structure – infrared: stars

1. Introduction

YSO (the acronym for Young Stellar Object) is a term widely used in the literature to indicate a star in the earliest phases of its evolution, when it is still intimately connected with the material from which it originated. The key characteristic of a YSO of interest for the present work is that the star is still surrounded by a dusty envelope or disk, which absorbs the stellar radiation, obscuring it in the visible range, and re-emits it in the IR, thus strongly modifying the input stellar spectrum and producing an observable IR excess.

YSOs may have masses from a fraction of a solar mass to one hundred solar masses, and consequently the luminosities will vary by more than six orders of magnitude. However, the acronym used remains the same, even though it will refer to entirely different classes of stars according to the stellar mass or luminosity.

For instance, for YSOs associated with luminous early type stars (earlier than B3), the gas-dust envelope surrounding the star will emit both in the radio continuum, due to the free-free emission of the ionized gas (HII region), and in the Middle and Far IR (MIR and FIR, respectively), due to the dust either inside the HII region or in the surrounding molecular cloud. Many detailed multi-frequency studies of very bright HII regions have amply exploited this field of research (for a review paper see e.g. Churchwell 1991) and models have been developed (especially for the earliest spectral types) that can explain the Spectral Energy Distribution (SED) from the radio to the FIR and the observed spatial morphology of the emission at different frequencies (see e.g. Scoville & Kwan 1976, Rowan-Robinson 1980, Churchwell et al. 1990, Ivezić & Elitzur 1997, Faison et al. 1998, Miroshnichenko et al. 1999).

For later spectral types (later than B3) the radio emission (or the stellar supply of Lyman continuum photons) decreases sharply and only the IR and sub-mm emission may be observ-

Send offprint requests to: M. Felli (mfelli@arcetri.astro.it)

⋆ This is paper no. 8 in a refereed journal based on data from the ISOGAL project

⋆⋆ Based on observations with ISO, an ESA project with instruments funded by ESA Member States (especially the PI countries: France, Germany, the Netherlands and the United Kingdom) and with the participation of ISAS and NASA

⋆⋆⋆ Table 4 is only available in electronic form at the CDS via anonymous ftp to cdsarc.u-strasbg.fr (130.79.128.5) or via http://cdsweb.u-strasbg.fr/Abstract.html

Table 1. Mean FIR to 5 GHz flux density ratio of HII regions (Felli et al. 2000)

λ/μm	$\langle$ LogF$_{FIR}$ - LogS$_{5GHz}$ $\rangle$	σ
12	1.86	0.52
25	2.62	0.53
60	3.70	0.51
100	4.05	0.57

able. In the range of luminosities between $\sim$10 and 10^3 L$_\odot$, the YSOs are better known as Herbig Ae/Be stars and the IR excess will come from a disk, an envelope or a combination of the two (see e.g. Berrilli et al. 1992, Hillenbrand et al. 1992, Pezzuto et al. 1997).

The YSOs of even lower luminosity, of the order of one solar luminosity, are called the T Tauri stars. In the widely adopted classification of YSO spectra the earliest phases are called Class 0 and Class I and have considerable IR emission (André et al. 1993; Lada & Wilking 1984; Lada 1999 and Natta 1999 for recent review papers).

Finally, YSOs of even lower luminosity and with masses in the brown dwarf range have recently been observed in the MIR (Olofsson et al. 1999).

The interesting aspect of YSOs is that, even though the spread of luminosities is very large, the SED of the excess emission in the IR (and the MIR colours) are rather similar. This comes from the fact that the MIR emission is produced by the same mechanism, i.e. re-radiation at lower temperature of the stellar emission absorbed by the dust. Consequently the colour will little depend on the luminosity, but on the overall optical depth in the dust envelope (Ivezić & Elitzur 1997). This common characteristic of YSOs will be the basic tool which we will use to separate YSOs from the much larger population of Post-MS stars in the Galactic Plane, which also have some IR excess due to dust in a circumstellar envelope produced by mass loss, but with slightly different colour.

The main goal of the present work is to establish general criteria that will allow us to identify YSOs in the ISOCAM observations of the Galactic Plane carried out during the ISOGAL program. ISOGAL observed scattered regions in the Galactic Plane at 7 and 15 μm (Pérault et al. 1996, Omont et al. 2000). The criteria are derived from existing ISOCAM observations as well as from theoretical indications and are tested on five Galactic fields at l $\sim$ +45°, observed during the ISOGAL program in the two broad band filters LW2 (5.5–8.5 μm) and LW3 (12–18 μm).

To avoid saturation effects, the ISOGAL fields were designed to exclude strong IRAS sources. As a result of this limitation, usually no IRAS source with F$_{12\,\mu m} \geq 6$ Jy should be present in the ISOGAL fields observed with broad band filters. The net result of this observational constraint is that we are bound to explore sources with relatively low flux densities, not accessible by IRAS, namely from the $\sim$ 10 mJy limit of the ISOGAL data at 15 μm to the upper limit quoted above. Because of the unknown distance this limitation does not translate directly into luminosities, but, on the average, ISOGAL observations should be able to detect either (few) intrinsically luminous but very far YSOs or (many) lower luminosity YSOs close to the Sun. Indeed, ISOGAL observations also avoided nearby low-mass star forming regions. They should thus be able to reveal solar mass YSOs at 1–2 kpc or intermediate mass YSOs up to the Galactic Centre.

2. The [15] magnitude versus [7]–[15] colour diagram and the colours of YSOs

We shall now explore the location of different types of objects in the [15] - [7]-[15] diagram to see how YSOs can be separated from other types of stars (cf. Fig. 1).

2.1. High luminosity YSOs

Felli et al. (2000) have examined a sample of 263 HII regions from the Galactic Plane survey of Becker et al. (1994) which were detected both in the radio with the VLA and in the FIR with IRAS. The mean ratios of the FIR to the 5 GHz flux density Log(F$_{FIR}$/F$_{5\ GHz}$), averaged over the entire sample, are given in Table 1 for the four IRAS bands.

A power law extrapolation of these values at 7 and 15 μm gives the following relations:

$$Log(F_{7\,\mu m}/F_{5\ GHz}) = 1.35 \pm 0.5 \quad (1)$$

and

$$Log(F_{15\,\mu m}/F_{5\ GHz}) = 2.0 \pm 0.5 \quad (2)$$

These relations should hold for the stars with the earliest spectral types (earlier than B0) which are the brightest and most easily detectable at 5 GHz with the VLA and with IRAS. For later spectral types we expect the ratios to be greater, since the ionizing flux and consequently the radio emission decreases rapidly with spectral type, while the IR emission should be less affected. We also remark that these relations hold only for the evolutionary phase of a luminous YSO in which a well developed HII region is present. For even earlier phases, if the radio emission is strongly self absorbed and/or the input luminosity comes from accretion, the ratio can change in a way that is difficult to predict.

The conversion from flux densities (in mJy) to magnitudes for the LW2 and LW3 filters (Blommaert 1998) are:

$$F_{7\,\mu m}/mJy = 9.03\ 10^4\ 10^{-0.4[7]} \quad (3)$$

$$F_{15\,\mu m}/mJy = 1.98\ 10^4\ 10^{-0.4[15]} \quad (4)$$

where [7] and [15] are the magnitudes at 7 and 15 μm respectively. The [7]-[15] colour is given by:

$$[7] - [15] = 1.65 - (LogF_7 - LogF_{15})/0.4 \quad (5)$$

With the use of the two previous relations (Eqs. (1)-(2)) it becomes [7]-[15] = 3.3 $\pm$ 1.

If we use relation (2) for 15 μm at face value we obtain the correspondence between MIR and radio flux densities for

Table 2. 5 GHz and 15 μm flux densities of HII regions derived from Eq. (2)

F_{15}/mJy	[15]	F_{5GHz}/mJy
12.5	8.00	0.125
100	5.74	1.0
250	4.75	2.5
1000	3.24	10.0

HII regions, shown in Table 2, which clearly illustrates that ISOGAL observations go much deeper than radio observations in detecting YSOs associated with HII regions. In fact, in the survey mode the VLA sensitivity is $\sim$ 2.5 mJy.

That this is the appropriate range of colours for HII regions is also confirmed in the ISOGAL field at (l,b) = (-0.27, -0.03) discussed by Schuller et al. (2000). Out of a much larger population of AGBs, there are 10–20 sources which could correspond to radio HII regions. All are clearly displaced from the rest in the [15] - [7]-[15] diagram, with colours [7]-[15] larger than 2 and with [15] $\leq$ 4.

2.2. Intermediate luminosity YSOs

Hillenbrand et al. (1992) have examined a large sample of Herbig Ae/Be stars and classified them into three groups. For Group I the IR excess is interpreted as coming from a disk and the SED for $\lambda \geq 2\,\mu$m is $\lambda F_\lambda \sim \lambda^{-4/3}$, which translates into [7]-[15] = 1.37. Group II has a higher IR excess and is best interpreted as young, intermediate-mass stars or star/disk systems surrounded by gas and dust which is not confined to a disk. From the observed SED the [7]-[15] colour is estimated to be 3 ± 0.4. Finally, Group III stars do not have IR excess and have very low MIR flux densities. They could be young, intermediate-mass stars which lack disks and which may be the higher mass analogous of disk-less T Tauri stars. For these stars [7]-[15] is lower than 0.9. Note that the Hillenbrand et al. (1992) classification is not consistent with the widely adopted classification for low mass YSO SEDs.

2.3. Low luminosity YSOs

Selected nearby star forming regions far from the Galactic Plane (in Chamaleon, Ophiucus, Serpens, Corona Australis) have been observed with ISOCAM in the same two filters (LW2 and LW3) by Olofsson et al. (1996), Nordh et al. (1998), Bontemps et al. (1998) and Olofsson et al. (1999). These fields are less crowded by evolved stars, more rich in low luminosity YSOs and field stars suffer lower line-of-sight extinction than typical ISOGAL fields. In all cases they find a clear dichotomy in the [15] - [7]-[15] diagram between sources with and without IR excess. The former (YSOs) have [7]-[15] between 1 and 2, while the latter have [7]-[15] around 0. To discriminate between the two types of sources they use values of [7]-[15] between 0.5 and 0.9, independent of the magnitude. In RCrA the derived luminosities imply masses in the range of brown dwarfs.

Similarly, using the SED of the four classes of YSOs we can see that Class 0 objects (the least evolved) have [7]-[15] $\geq$ 10, Class I [7]-[15] $\sim$ 3, Class II [7]-[15] $\sim$2.2 and Class III [7]-[15] $\leq$ 1 (André et al. 1993; Lada & Wilking 1984; Lada 1999). These are the more evolved, with little IR excess and, consequently, we do not consider them as YSOs.

2.4. Models of dusty envelopes around young stars

An alternative and independent way to estimate the expected colour of YSOs is to use the results of SED modelling presented in the literature.

Faison et al. (1998) recently modelled the SED of dusty HII regions. From the published fits to the observations we have derived the flux densities at 7 and 15 μm for the envelopes surrounding two stars of different spectral types: an O5.5 (T_{eff} = 44840 K) and a B0 (T_{eff} = 33400 K). In both cases the [7]–[15] colours are similar and $\sim$1.8. Variations around this value are expected depending on the parameters of the dust envelope (temperature at the inner and outer parts of the envelope, density profile, inner and outer radius, etc) and the varying extinction along the line of sight.

In order to construct a consistent set of colours and magnitudes expected for a wide range of YSO luminosities, we used the DUSTY[1] code (Ivezić & Elitzur 1997) to solve for the SED emerging from a spherical dusty envelope around a young stellar source. Faison et al. (1998) and Miroshnichenko, Ivezić & Elizur (1997) showed that the infrared part of the SED of high and intermediate luminosity YSOs is well represented by a central ZAMS stellar source surrounded by a spherical envelope with a shallow density profile and an overall optical depth in the range $1 \leq \tau_V \leq 100$. Using the stellar parameters (L_*, T_{eff}) from Schmidt-Kaler (1981), a 1.5 index power law density profile for the dusty envelope and an overall optical depth at V ranging from 1 to 100, we computed the emerging spectra for central stars with spectral type in the range from G0 to O6. The [7] and [15] magnitudes were then obtained convolving the computed spectra with the LW2 and LW3 band profiles, after scaling the computed spectrum to have the correct total luminosity at a fiducial distance. In all cases the colours are in the range 1.5$\leq$[7]–[15]$\leq$1.8. However, note that adding external extinction from cold (i.e. non emitting in the mid-infrared) dust along the line of sight (either in the YSO's parental cloud or in the plane of the Galaxy) will move the colours to higher values.

2.5. Late type Post MS stars

In order to establish the region of the [15] - [7]-[15] diagram populated by late type Post-MS stars with IR excess (AGBs and long period Mira Variables) we refer to ISOGAL fields observed in the Galactic Bulge in two windows of low extinction (the Baade's Windows, Glass et al. 1999) and in the intermediate Galactic Bulge (Omont et al. 1999a). These fields have a low

[1] DUSTY is available on the www at: http://www.pa.uky.edu/$\sim$moshe/dusty

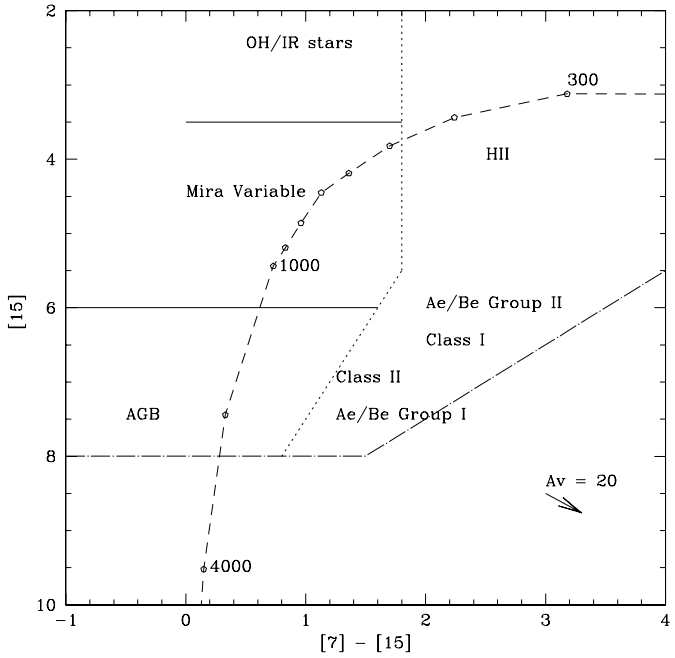

Fig. 1. The [15] - [7]-[15] diagram. The short-dashed line gives the proposed separation between YSOs (to the right) and evolved stars (to the left). The location of different types of objects is indicated. The long-dashed line gives the position in the diagram of a 10 $L_\odot$ black-body placed at the distance of 1 kpc (or 10^3 $L_\odot$ at 10 kpc) with temperatures 300, 400, 500, 600, 700, 800, 900, 1000, 2000, 4000 K marked by circles. The arrow in the lower right indicates the displacement for A_v = 20. The dot-dashed line defines the region of confidence imposed by the conditions [7] $<$ 9.5 and [15] $<$ 8 magnitudes.

amount of galactic interstellar matter along the line of sight (Av $\sim$ 2 for the Baade's Windows and Av up to 7 for the intermediate Galactic Bulge) and hence a low expected presence of YSOs, but, at the same time, are richly populated by Post-MS stars.

The sources observed by ISOCAM in the two filters are all evolved stars and are located in a sligthly inclined strip of the [15] - [7]-[15] diagram which represents a sequence of increasing 15 μm dust emission: the mean [7]-[15] colour is $\sim$ 0.2 at [15] = 9 and increases to 1.4 at [15] = 5. The region with higher magnitudes ([15] $\geq$ 6) is populated by late type M-stars on the AGB, the region with lower magnitudes ([15] $\leq$ 6) by Mira variables. For even lower magnitudes ([15] $\leq$ 3.5) association of ISOGAL sources with OH/IR stars has been found (Schuller et al. 2000, Ortiz et al. 2000).

2.6. A schematic separation of sources in the [15]-[7]-[15] diagram

From all the indications presented in the previous sections the position of different types of stars in the [15] - [7]-[15] diagram is summarized in Fig. 1.

For the separation between AGBs and intermediate luminosity YSOs (Class II and Ae/Be of Group I) we have adopted an inclined line, from (mag, col) = (0.4, 9) to (mag, col) = (1.8, 5.5) to take into account the inclined strip of AGBs. For lower magnitudes ([15] $\leq$ 5.5) the separation between Mira Variables and OH/IR stars from HII regions, Ae/Be Group II and Class I YSOs is taken as the vertical line at [7]-[15] = 1.8 (see Schuller et al. 2000).

This dividing line is quite different (and more conservative) than that adopted by Olofsson et al. (1999) for the RCrA field ([7]-[15] = 0.5) or Nordh et al. (1998) for nearby star forming regions ([7]-[15] = 0.9). Had we used their criteria the number of possible YSOs in our fields would have been almost an order of magnitude greater and comparable to that of evolved stars. Clearly, their criteria are applicable only in fields where the density of evolved stars is much smaller than that of YSOs and the extinction along the line of sight is very low.

The intrinsic colours and 15 μm magnitudes may be altered by interstellar extinction. The arrow in the lower right in Fig. 1 indicates the shift for A_v = 20, assuming the very uncertain relations A_7 = 0.028 A_v and A_{15} = 0.015 A_v found by Jiang et al. (2000) in the ISOGAL field at (l,b) = (-18.63+00.35). The effect of extinction may be important and has then to be taken into account before attempting any separation into different classes of objects as illustrated in the heavily extincted ISOGAL field at (l,b) = (-0.27, -0.03) (Schuller et al. 2000), where the entire AGB sequence seems shifted to the right.

In Fig. 1 the colour and [15] magnitude of a black-body with luminosity of 10 $L_\odot$ at a distance of 1 kpc and with temperatures from 300 K to 4000 K is shown for comparison. MS stars with no IR excess have [7]-[15] $\sim$ 0.

The dot-dashed line in Fig. 1 limits the region of confidence in the [15] - [15]-[7] diagram (the upper left) resulting from the limits [7] $<$ 9.5 and [15] $<$ 8 magnitudes, which will be discussed in Appendix A.

It is obvious that the suggested separation between YSOs and late type stars is rather artificial. Contamination of the two areas in which we have divided the [15] - [7]-[15] diagram from objects of the other type is expected due to several independent causes: 1) errors in the observed magnitudes (which will be discussed in the next section), 2) unknown correction for extinction; this effect will be particularly important since the population of evolved stars in the Galactic Plane is much larger than that of the YSOs, and 3) intrinsic spread of the colours. In fact, the colour is a sensible function of YSO evolutionary status, of the geometry of observations for disks inclined with respect to the line of sight, and of chemical differences. However, the adopted separation should be sufficient, especially on large samples, to provide a first list of possible YSOs, to be further confirmed by additional observations in other bands or spectroscopy.

An estimate of the contamination from evolved stars using the above criteria can be obtained using the ISOGAL results toward the Baade's Windows (Glass et al. 1999). The total number of objects detected at both 7 and 15 μm above our confidence levels in the two Baade's window fields is 224, no extended MIR sources are detected in these fields. Out of the 224 sources 11 would be selected as YSOs using our colour criteria, none of which with [15] $<$ 5. All the 11 sources but one are very close to the separating line. Under the extreme assumption that

the two Baade's Window fields do not contain *any* YSO, the maximun contamination using our selection criteria is $\leq 5\%$. The contamination will be very strong close to the separating line but will be increasingly less important farther to the right of the separating line.

Finally we note that Class 0 YSOs (André et al. 1993) will not be detected in our survey because they are too heavily extinguished to be observed at 7 or 15 μm.

3. The ISOGAL observations

The complex data reduction procedure used to produce the ISOGAL images from the ISO observations with ISOCAM are described in Pérault et al. (1996) and Omont et al. (1999a) for the most recent procedures (see also Glass et al. 1999 and Omont et al. 1999b).

Point sources are extracted from the ISOGAL images with a specific program written by C. Alard at IAP. This program first re-samples the image on a finer grid, then determines an analytic expression of the point spread function (PSF) by analyzing the brightest sources in each image. Then it finds sources by maximizing the correlation with the PSF. Once detected, sources are extracted by means of least square PSF fit. The method starts with the brightest sources, removes them, and follows iteratively to the fainter ones. This is a powerful method, even in crowded fields, since it is able to extract overlapping sources correctly. However, at this stage an extended source cannot be extracted.

After the elimination of the false replication sources due to memory effects of the receivers (see e.g. Omont et al. 1999a, appendix B.1), the two lists of point sources (7 and 15 μm) are then cross-correlated to provide a single list that contains sources detected in the two filters and sources detected only in one filter. This list is saved in the ISOGAL archive. The lists are then edited for non perfectly matching edges of the fields in the two filters, eliminating sources detected only in one filter because they are outside the observed field in the other filter. Sources too close to the border of the fields are also eliminated.

4. The ISOGAL fields at l = +45°

The choice of the ISOGAL fields at l = +45° for a first analysis of the YSO content is motivated by the desire to find a region representative of a typical situation in the plane: i.e. not overcrowded by evolved stars, not too strongly extincted and not centered on a well known star forming region. Moreover, this region had been expressly observed in the radio with the VLA at 3.6 and 6 cm by Testi et al. (1999, hereafter TFT) in order to have comparison radio observations.

A total of 34 discrete radio sources were detected by TFT, 13 of which clustered in five separate extended complexes. The 5 complexes were all multiple or single extended thermal HII regions. For each of these complexes a bright IRAS counterpart could be found and the IRAS colours satisfy the Wood & Churchwell (1989; WC89) criteria for HII regions. No IRAS counterpart could be identified for any of the remaining 21 radio sources. According to the radio spectral index six of these are candidate UC-HII regions, while the other 15 are most probably background extragalactic non-thermal sources.

Observations at other radio wavelengths and resolutions will also be used when available. In particular, we shall make extensive use of the 1.4 GHz NRAO VLA Sky Survey (NVSS – Condon et al. 1998). The NVSS used the most compact VLA configuration (D array) with a flux density limit of ~ 2.5 mJy/beam (~ 0.5 mJy/beam rms) and an angular resolution of $\sim 45''$.

The flux density limit in NVSS and TFT are both ~ 2.5 mJy and correspond to [15] $\sim$ 4.75 (see Table 2). Consequently, there should be many YSOs in the ISOGAL fields which do not have a radio counterpart and, conversely, any radio-identified HII region should have a bright MIR counterpart.

The basic tools that will be used to identify the YSOs from the much larger population of stellar objects present in the ISOGAL fields will be:

1. For point MIR sources we shall select YSOs on the basis of their position in the [15] - [7]-[15] diagram and, for the brightest ones, on the correspondence with thermal radio sources. In this context it must be noted, as will be made clear in the analysis of individual fields, that only a subset of the ISOGAL sources are detected in both filters. A large number of sources are detected at 7 μm only, with a smaller fraction at 15 μm only. This is an effect due to the intrinsically different SEDs of the sources. The following discussion will concentrate primarily on the sources detected in the two filters. Those detected only at 7 μm will not be considered in our analysis because most probably they are evolved stars. We shall retain in the analysis those detected only at 15 μm when the lower limit to the colour brings them into the region of the YSOs.
2. For the extended sources in the ISOGAL fields we shall rely on a morphological comparison with available radio interferometric observations.

The parameters of each of the five ISOGAL fields are given in Table 3, where a conventional short name (A-7 to E-7 and A-15 to E-15) has been introduced for simplicity. The other columns contain: 2) the galactic coordinates of the centre of each field 3) Orbit-frame: the first three digits are the ISO orbit and

Table 3. Parameters of ISOGAL fields

Field	Name	Orbit-Frame	dl	db	r.a.	dec	Filter
A-7	+44.99+00.73	48300172	0.10	0.15	19.18	11.05	LW2
A-15	+44.99+00.73	72101803	0.10	0.15	19.18	11.05	LW3
B-7	+44.99+00.35	48300274	0.18	0.17	19.21	10.88	LW2
B-15	+44.99+00.35	13901157	0.18	0.17	19.21	10.88	LW3
C-7	+44.99−00.21	48300173	0.18	0.30	19.24	10.62	LW2
C-15	+44.99−00.21	13900956	0.18	0.30	19.24	10.62	LW3
D-7	+45.23−00.32	48300175	0.14	0.13	19.25	10.78	LW2
D-15	+45.24−00.30	13901159	0.13	0.15	19.25	10.80	LW3
E-7	+44.95−00.75	48300276	0.10	0.15	19.27	10.33	LW2
E-15	+44.95−00.75	72101804	0.10	0.15	19.27	10.33	LW3

the last five the number of the frame, 4) and 5) the approximate extension (half-length and half-width) of the field in (l,b), 6) and 7) J2000 right ascension (in hours) and declination (in degrees) of the field centre, and 8) the filter used.

A graphical view of the five observed fields in galactic coordinates is given in Fig. 2, where the grey scale images are the 15 μm ISOGAL observations, the grey contours represent the radio sources from the NVSS and the crosses the positions from TFT. It is clear that several bright and extended radio sources (most of them HII regions) are just outside the edge of the ISOGAL fields (for example between fields B and C). This results from avoiding IRAS sources with $F_{12\,\mu m} \geq 6$ Jy.

The full contours are from the CO(1−0) survey of the Galactic Plane (Dame et al. 1987). The CO(1−0) data indicate that our fields are not coincident with a peak in the CO emission and that field A is in a region totally devoid of noticeable CO emission. Consequently, given the small molecular column density, the extinction should be moderate and the expected abundance of YSOs not particularly high.

4.1. Evaluation of accuracy of the ISOGAL observations

The general characteristics and quality of the ISOGAL data have been discussed in various fields, especially through repeated independent observations of the same regions (Pérault et al. 1996, Omont et al. 1999a, Glass et al. 1999, Omont et al. 1999b, Ganesh et al. in preparation, Ojha et al. in preparation). Among the observations of the fields at l $\sim$ +45°, the LW2 and LW3 observations of fields C and D which are partly overlapping also offer this possibility (see Appendix A). However, this overlapping area is relatively small and a large part of it is at the edge of one of the rasters, where the data are of inferior quality because near such edges a sky position is observed only once, instead of twice.

The results of all these discussions are rather consistent. A good degree of completeness and reliability is generally achieved for $[7] < 9.5$ and for $[15] < 8$.

The photometric accuracy is estimated from repeated observations and retrieval of artificially added sources. The typical rms is ∼0.2–0.3 mag. This increases for the weakest sources and in edge regions such as a part of the overlapping area of fields C and D. Systematic biases of ∼0.1–0.2 mag are still possible because, in particular, of the difficulty of the correction of transient effects. Biases can reach 0.3–0.5 magnitude in particular fields where defects of data processing are not yet corrected (Schuller et al. 2000).

We conclude that the confidence limits are $[7] = 9.5$ and $[15] = 8$. The sensitivity limits of the ISOGAL observations are nearly one magnitude greater, but the confidence at such faint magnitudes is lower. The photometric errors can reach 0.3–0.4 magnitude even for sources one magnitude brighter than the confidence limit. They can be greater close to the edges of the fields and for sources close to the confidence limit or fainter; they can even be of the order of 1 magnitude for faint sources close to the edges (see also Appendix A.).

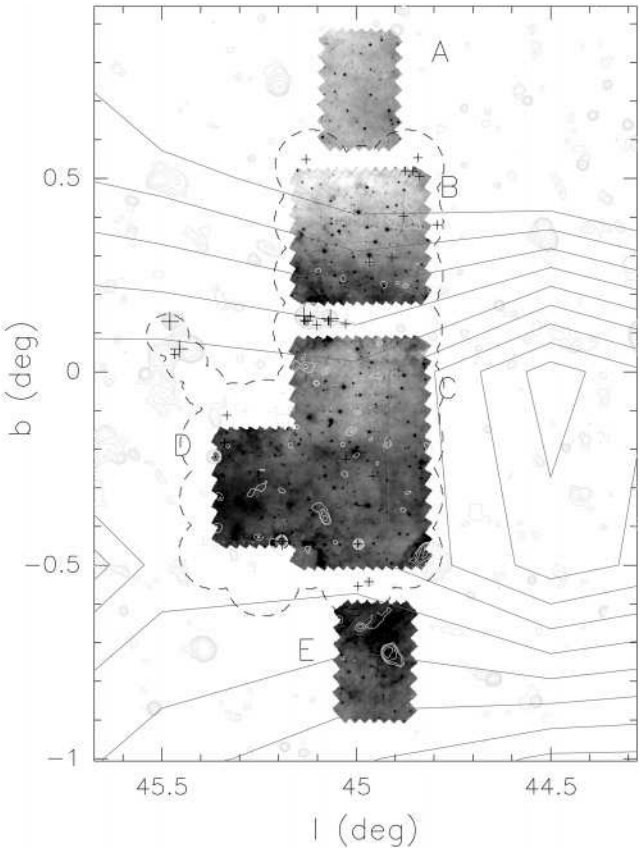

Fig. 2. The five ISOGAL fields at 15 μm (grey scale). The grey contours represent the radio sources from the NVSS and the crosses the positions of the radio sources from TFT. The full contours are from the CO(1−0) survey of the Galactic Plane (Dame et al. 1987), the dashed contour the area observed by TFT.

4.2. Description of the individual fields

In Fig. 3 we show the colour-magnitude and magnitude distributions for each of the five fields. In the plots we also include sources with [7] > 9.5 and [15] > 8, although we will not consider them in the discussion.

The two right columns give the distribution of sources as a function of the [7] and [15] magnitudes. The solid line gives the sources detected at both wavelengths, the short dashed line those detected only at 7 or 15 μm, respectively.

The left column give the [15] magnitude versus [7]-[15] colour. The crosses represent the sources detected at both wavelengths, the right arrows those detected only at 15 μm and represent lower limits to the true colour (i.e. the point should be moved to the right) assuming [7] = 9 magnitudes. In Table 4 we list for all fields (with no overlap) the sources that satisfy our confidence criteria, i.e. [7] $\leq$ 9.5 and [15] $\leq$ 8, as well as those detected only at 15 μm and with lower limit to the colour to the right of the dashed line. Table 4 contains name of the source[2],

[2] Following the standard format agreed with CDS the name is ISOGAL-PJhhmmss.s+ddmmss, where P stands for Provisory, J for equinox J2000, hhmmss.s hours, minutes and seconds of right ascension, ddmmss degrees, minutes and seconds of declination

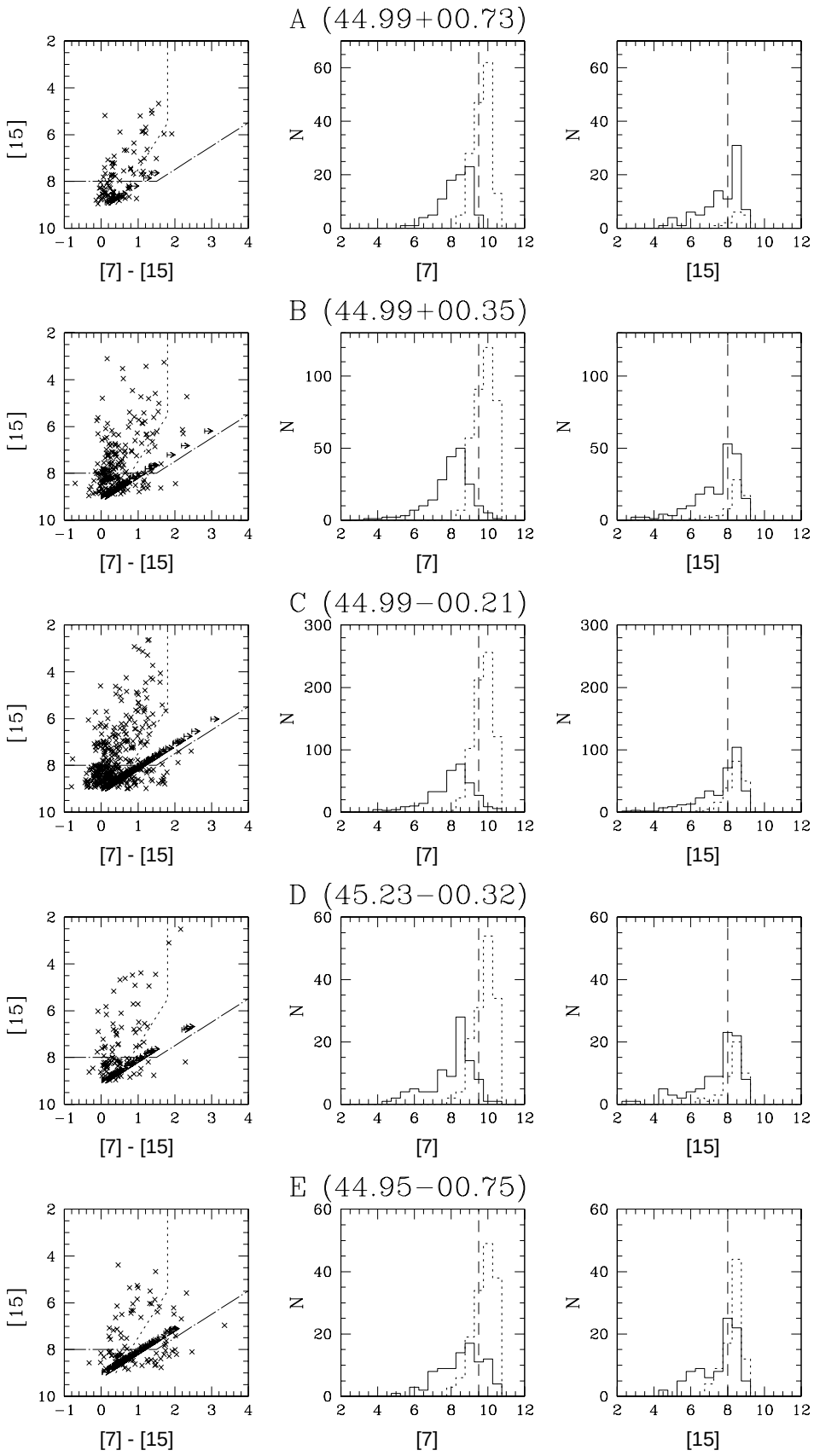

Fig. 3. Colour-magnitude diagrams and magnitude distributions for each ISOGAL field, from top to bottom: field A (44.99+00.73), field B (44.99+00.35), field C (44.99–00.21), field D (45.23–00.32), and field E (44.93–00.75); left column: [15] vs. [7]–[15] colour magnitude diagram, dotted and dot-dashed lines as in Fig. 1; central column: [7] magnitudes distributions; right column: [15] magnitudes distributions, in both diagrams the full line gives the sources detected at 7 and 15 μm, and the dotted line those detected only at 7 or 15 μm, respectively. The vertical dashed lines give the adopted confidence limits [7] = 9.5 and [15] = 8.

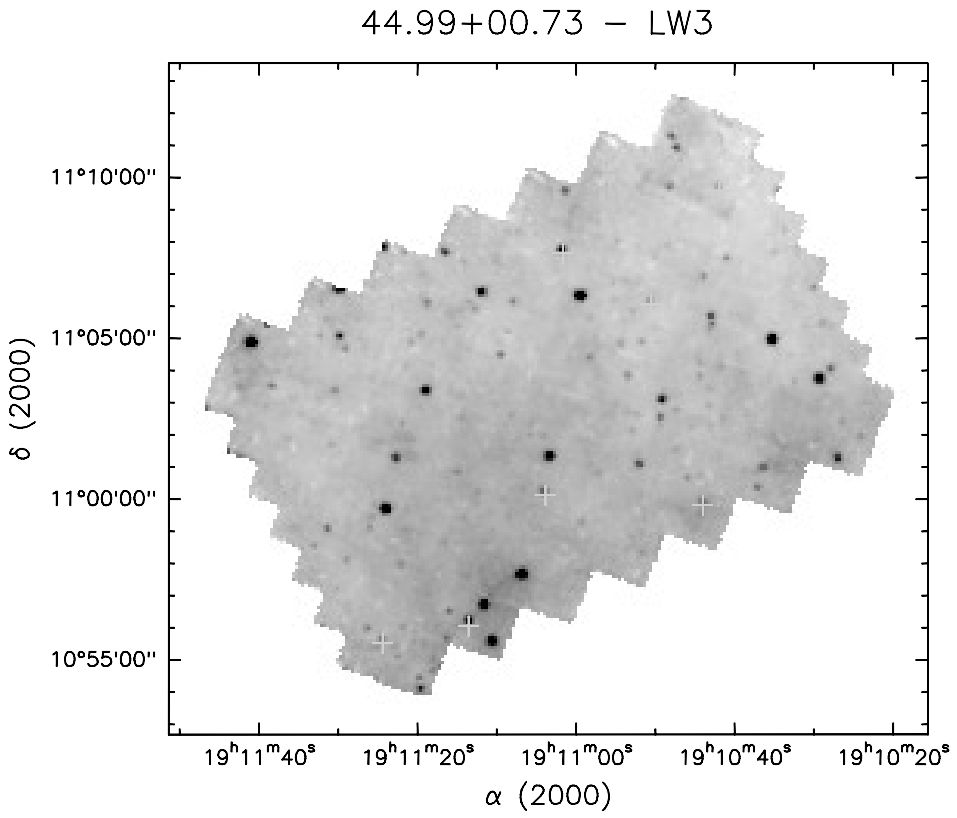

Fig. 4. Field A (44.99+00.73). The 15 μm image with YSOs marked with a cross.

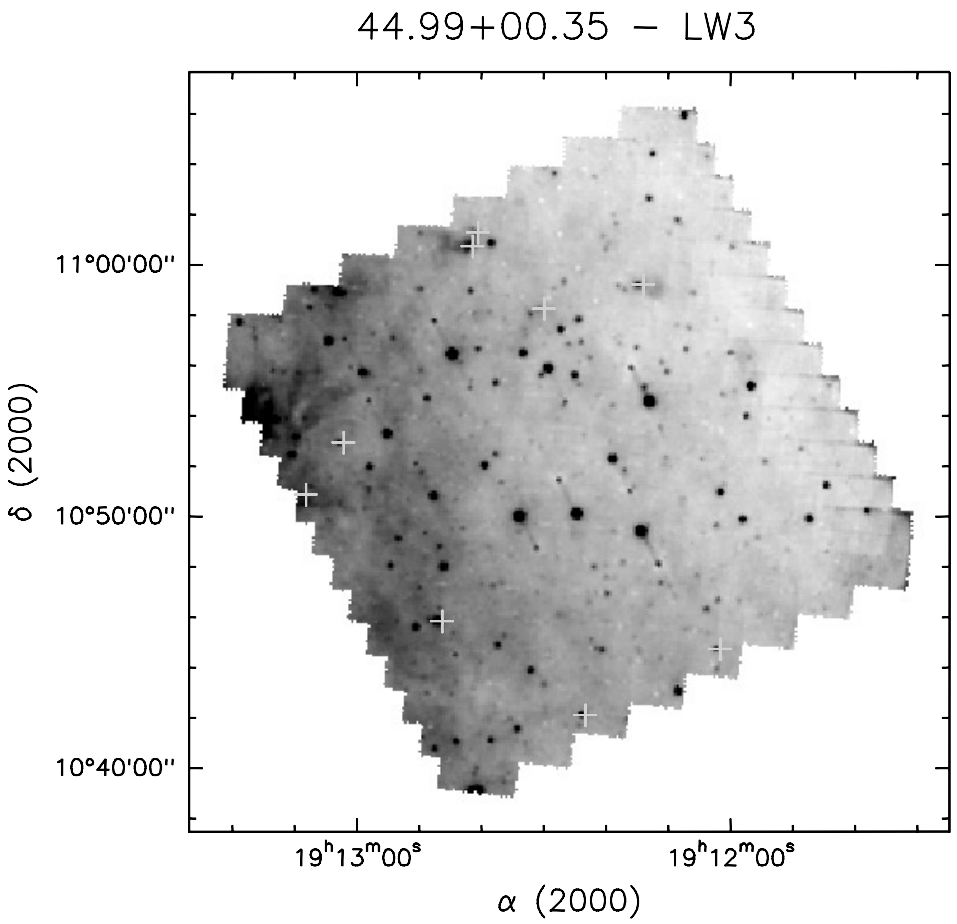

Fig. 5. Field B (44.99+00.35). Caption as in Fig. 4.

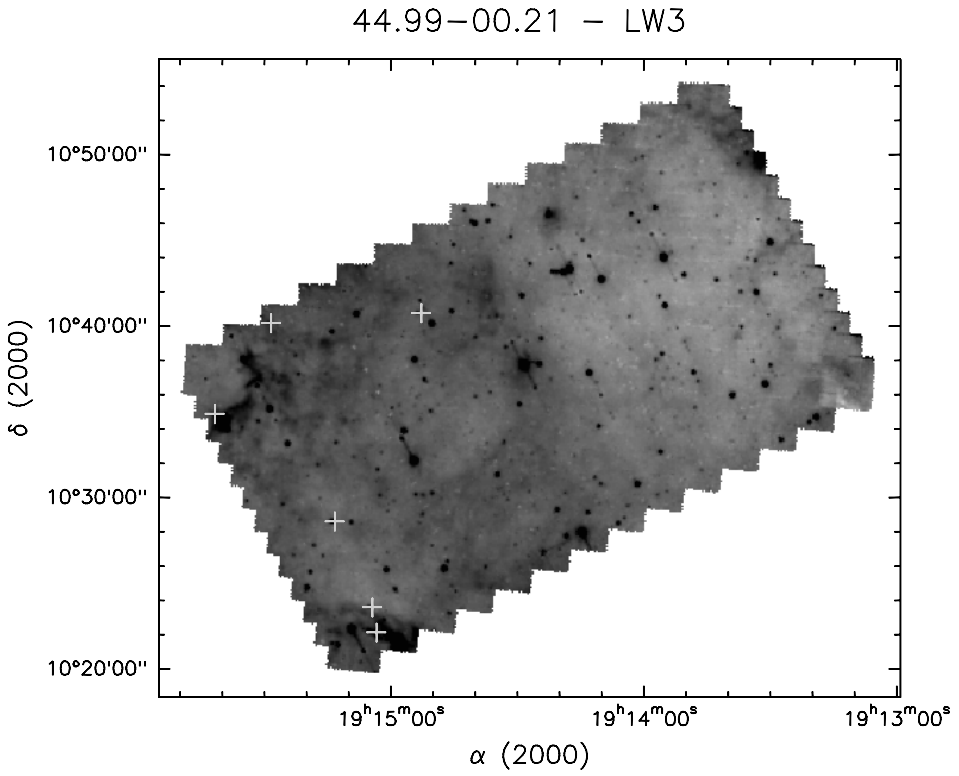

Fig. 6. Field C (44.99-00.21). Caption as in Fig. 4.

7 and 15 μm magnitudes and an identification code: 1) "YSO", for those detected at 7 and 15 μm and with colour to the right of the dashed line, 2) "cYSO" (candidate YSO) for those detected only at 15 μm and with lower limit to the colour to the right of the dashed line.

4.2.1. Field A (44.99+00.73)

In Fig. 4 we show the 15 μm image with only the YSOs marked with a cross.

Comments:

1. The number of sources detected in both filters above the confidence limits is 44.
2. In this field the percentage of sources detected only at 15 μm is the smallest of the five fields considered.
3. There are 7 YSOs, none of which with [15] $\leq$ 5.
4. There are 2 cYSOs.
5. There is no TFT radio source (but the overlap with the area covered by TFT is marginal, see Fig. 2) and no NVSS source.
6. There are no extended structures which may mimic diffuse extended HII regions.
7. The YSOs tend to be located in areas with stronger diffuse 15 μm emission.
8. The area covered is 0.058 square degrees.

In summary, all the indications (no radio source, no YSOs with [15] $\leq$ 5, small percentage of sources detected only at 15 μm, no extended structures) point out that this field is completely devoid of bright YSOs associated with HII regions and is populated by a small number of lower flux density YSOs. This is consistent with the location of Field A in a direction of very low CO column density, as indicated in Fig. 2.

4.2.2. Field B (44.99+00.35)

In Fig. 5 we show the 15 μm image of Field B, with the YSOs overlayed.

Comments:

1. The number of sources detected in both filters above the confidence limits is 112.
2. The sources detected only at 15 μm are a considerable fraction of the total detected at 15 μm.
3. There are 9 YSOs. Only the YSO with [15] $<$ 5 (ISOGAL-PJ191246.3+104551) coincides with a NVSS source which has a flux density of 4.3 mJy and is unresolved with a resolution of $\sim 45''$. This source also coincides with the H_2O maser reported by Testi et al. (1997). The coincidence with the NVSS source confirms the correctness of the previous interpretation of the ISOGAL source in terms of a star forming region. However, we do not find any radio counterpart in TFT. One possible explanation for this non detection by TFT is that the source is optically thin and slightly extended, making it too faint for the 3–6 $''$ resolution of TFT. Alternatively, it could be a non-thermal jet of the type found associated with the H_2O maser in W3(OH) (Reid et al. 1995).
   More sensitive VLA observations are needed to settle this point.
4. There are 8 cYSOs.
5. There are 4 thermal sources from TFT: 2,3,8 and 9. None of these has an ISOGAL counterpart. This is surprizing in

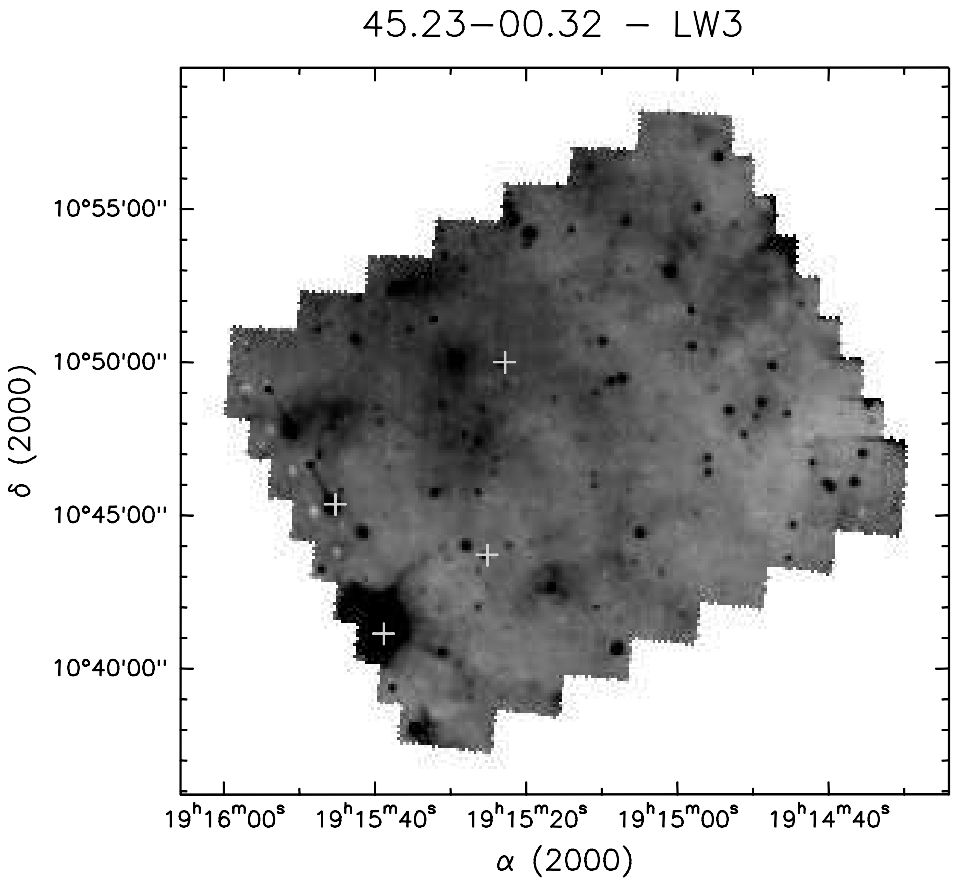

Fig. 7. Field D (45.23-00.32). Caption as in Fig. 4.

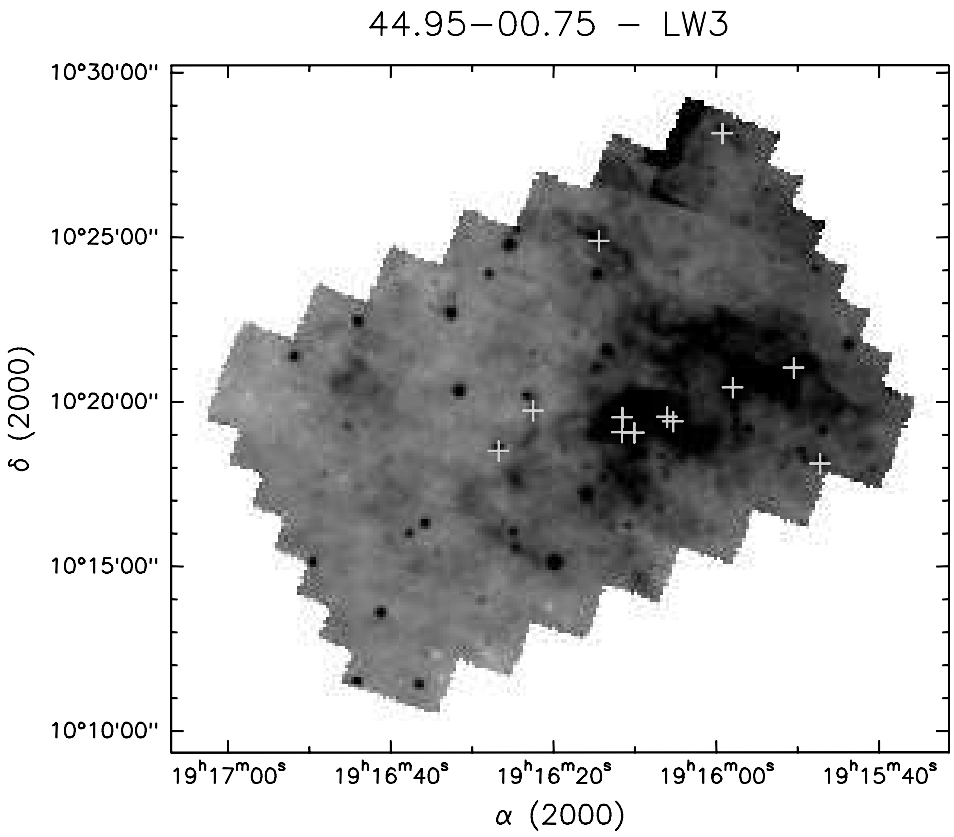

Fig. 8. Field E (44.95-00.75). Caption as in Fig. 4.

view of the discussion of Sect. 4. Source 9 has also been detected in the NVSS with a flux density of 3.3 mJy. Source 9 coincides with a weak "hole" in the background surface brightness distribution at 15 μm. The possible speculation is that source 9 is a very young source with extreme visual extinction, similarly to IRAS23385+6053 (Molinari et al. 1998).
6. The YSOs tend to be associated preferentially with diffuse features or small nebulosities in the 15 μm image.
7. The area covered by this field is 0.117 square degrees.

In summary, this field has one high flux density YSO identified from the radio correspondence (1.4 GHz only), its colour and the presence of an H_2O maser, and 8 YSOs of lower flux density.

4.2.3. Field C (44.99-00.21)

In Fig. 6 we show the 15 μm image of Field C, with the YSOs overlayed.

Comments:

1. The number of sources detected in both filters above the confidence limits is 153.
2. The number of sources detected only at 15 μm is comparable to that of sources detected at the two wavelengths.
3. There are 6 YSOs, none of which with [15] $\leq$ 5, nor with a radio continuum counterpart in the NVSS or in TFT. One of the YSOs (ISOGAL-PJ191528.4+104012) is in the region of overlap with Field D but it is not classified as a YSO in that field. However, the colour for this source is very uncertain due to its weakness ([7] = 8.9 and [15] = 7.9 magnitude). Two of the YSOs are embedded within a diffuse region at 15 μm partly visible in the lower corner, which is also detected in the radio continuum as an extended source by the NVSS and is mostly outside the area observed with ISO (see Fig. 2).
4. There are 34 cYSOs.
5. In TFT there are 3 sources (20,21 and 25), all non-thermal. None of these has an ISOGAL counterpart. Source 25 is also present in the NVSS.
6. There are 15 NVSS sources in the field, none of which shows coincidences with ISOGAL sources, except for the extended radio source at the south edge of the image (see also Fig. 2) which is only partly covered in the ISOGAL image.
7. Also in this case the YSOs tend to be associated preferentially with diffuse features or small nebulosities in the 15 μm image.
8. The area covered is 0.203 square degrees.

In summary, even though this field is centered on the Galactic Plane, there is only one extended HII region at the edge of the field, no bright YSO and a large number of low flux density YSOs and cYSOs.

4.2.4. Field D (45.23-00.32)

In Fig. 7 we show the 15 μm image of Field D, with the YSOs overlayed.

Comments:

1. The number of sources detected in both filters above the confidence limits is 37, considering only the region not overlapping with Field C. As in the previous field centered on the Galactic Plane, the number of sources detected only at 7 μm is overhelming.
2. The number of sources detected only at 15 μm is comparable to that of those detected at both wavelengths.
3. There are 4 YSOs: two are rather weak and two are very bright, with [15] = 2.5 and 3.1. The brightest YSO (ISOGAL-PJ191538.8+104109) is surrounded by extended MIR emission. It coincides with the thermal extended radio source 34 of TFT (see Fig. A6 of TFT) and has a NVSS counterpart. It is the best example of YSO identified with an HII region in our fields. The other bright YSO is point-like and close (though not exactly coincident with) a faint (4.5 mJy) NVSS source; this radio source is not detected by TFT.
4. There are 8 cYSOs plus one in the region overlapping with Field C.
5. The area covered is 0.070 square degrees.

In summary, this field contains a canonical example of an HII region, two high luminosity YSOs, one of which in the HII region, two lower flux density YSOs and 8 cYSOs.

4.2.5. Field E (44.95-00.75)

In Fig. 8 we show the 15 μm image of Field E, with the YSOs overlayed.

Comments:

1. The number of sources detected in both filters above the confidence limits is 40.
2. Even though this field is centered at b = -0.75°, its distribution of sources as a function of [7] and [15] magnitudes is more similar to those in the Galactic Plane than in its counterpart at b = +0.73°, i.e. a large abundance of sources detected only at 7 μm and similar numbers of sources detected only at 15 μm and at both wavelengths. We note that in this direction the CO emission is stronger than towards Field A (see Fig. 2).
3. The overlap with TFT is very small (see Fig. 2) and there is no thermal source.
4. There are 12 YSOs, none of which with [15] $\leq$ 5. None of these has a corresponding NVSS source. Almost all are surrounded by a diffuse nebulosity.
5. There are 21 cYSOs.
6. There are 7 NVSS sources in the field. One is located close to the top right corner, where a diffuse nebulosity is partly visible. In the central part of the 15 μm image there is a bright diffuse nebula, which corresponds to an extended source in the NVSS image (see Fig. 2). Five of the YSOs are located in close connection with this extended nebula. The source seems to be an extended HII region around a young stellar cluster.

Table 5. YSOs in the l = +45° fields

	A	B	C	D[a]	E	Total
Extended at 15 μm						
with radio emission	-	-	1	1	1	3
High luminosity YSO	-	1	-	2[b]	-	3
Low luminosity YSO	7	8	6	2	12	35
Candidate YSO	2	8	34	8	21	73
Total	9	17	41	13	34	114

[a] Only the part of Field D not overlapping with Field C is considered.
[b] One of the high luminosity point sources is within the extended source.

7. The area covered is 0.058 square degrees.

In summary, there is an extended MIR-radio HII region, 12 YSOs and 21 cYSOs.

4.3. Identified YSOs

The number of possible identified YSOs are summarized in Table 5.

The most secure identifications are the 3 high luminosity point-like sources associated with radio continuum emission. There are 3 extended sources associated with diffuse radio emission and classified as HII regions. There are 35 possible lower luminosity point-like YSOs (without radio emission). They may suffer some contamination at the higher [15] magnitudes and close to the separating line. Of the 35 only 7 are in this situation, while the rest are sufficiently far from the separating line to make contamination much less probable. The total number of objects detected at both bands above the stated confidence levels in the five ISOGAL fields is 386, thus the maximum contamination from reddened evolved stars is at most 19 objects if we use the 5% contamination derived for the Baade's Window fields. Follow-up near infrared and sub-millimiter observations are required to ascertain the nature of every single object in this sample. There are 73 candidate YSOs (detected only at 15 μm), by far the larger number. However, the weakest cYSOs need to be validated since residual artefacts, such as false replication sources due to remanence effects (Glass et al. 1999), are possible.

The histogram of YSOs and cYSOs as a function of the [15] magnitude, shown in Fig. 9, indicates that: 1) the number of identified YSOs decreases at brighter magnitudes, as expected, 2) for $6 < [15] < 7.5$ the two distributions have comparable values, 3) the cYSOs distribution has a large peak for sources close to the limiting magnitude, due to the loss at 7 μm of sources with [7]–[15]$\geq$1.5. It is clear that the classification of these sources is the most uncertain.

The number of HII regions identified by TFT is larger than that found by ISOGAL. This is because the TFT survey covers uniformly the region centered at l = + 45° and many of the radio identified HII regions lie outside the boundary of the ISOGAL fields, which were chosen to avoid bright IRAS sources. In particular, TFT identify five HII complexes (i.e. including extended and small diameter sources in the same area): (11 + 12 + 30), (13 + 15 + 16 + 17 + 31), (34), (18 + 33) and (32), and 6 isolated small diameter thermal sources: 2, 3, 8, 9, 19 and 22. Of the five HII complexes, only (34) is within the area covered by ISOGAL. Of the small diameter ones, 19 and 22 are outside the area covered by ISOGAL. We do not have an explanation for the lack of an ISOGAL counterpart to the thermal radio sources 2, 3, 8 and 9, apart from invoking extremely high visual extinctions of the type discussed by Molinari et al. (1998). In order to confirm this hypothesis submillimeter continuum observations and molecular observations in high density tracers are required.

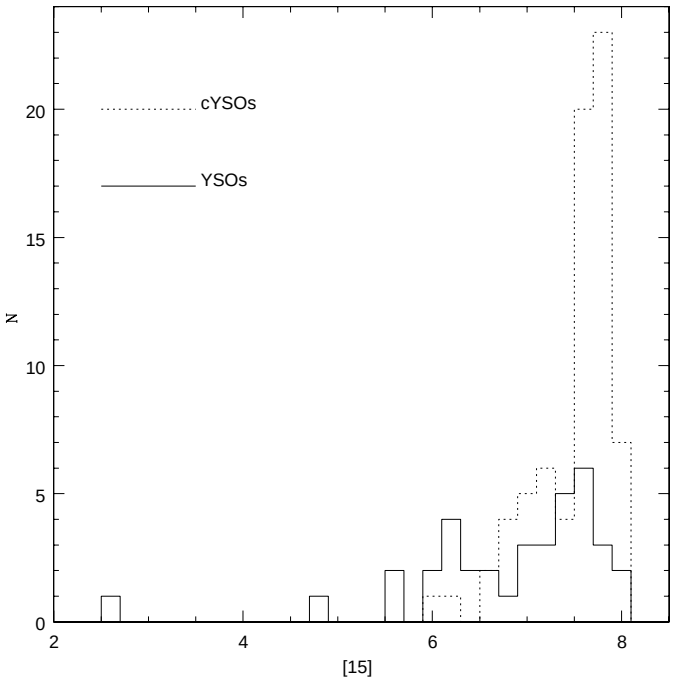

Fig. 9. Histogram of YSOs and cYSOs as a function of the [15] magnitude.

5. Discussion

5.1. Expected number of YSOs

Given the much greater sensitivity of ISOGAL with respect to IRAS it is interesting to compare the expected number of YSOs in the ISOGAL fields with the observed one in order to have an independent check on the validity of the adopted selection criteria.

Dealing with such a large range of luminosities, the first step is to find out the limiting distance at which a YSO can be detected with the ISOGAL sensitivity, as a function of its luminosity. For this it is important to know if the 7 and 15 μm fluxes scale linearly with the YSO luminosity.

For two close-by star forming regions (RCrA and Chamaleon scaled to the distance of RCrA, equal to 129 pc) Olofsson et al. (1999) find that the 7 μm flux density of identified YSOs scales linearly with luminosity for the range of luminosities of their samples, i.e. for $-2 < \mathrm{LogL/L_\odot} < 1.5$. The relation is:

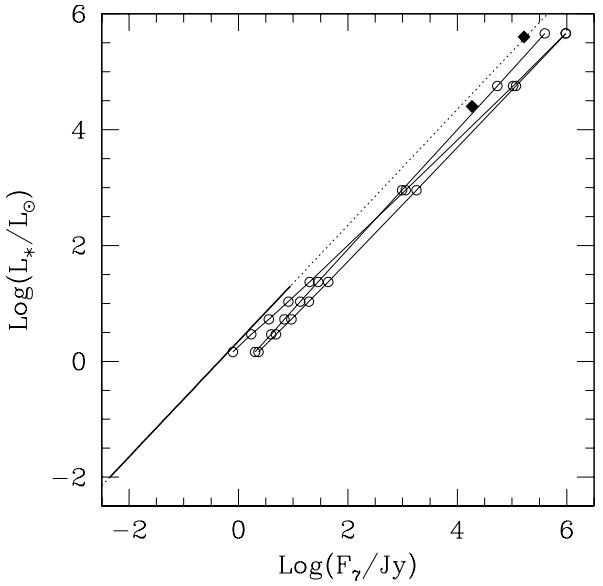

Fig. 10. Luminosity versus 7 μm flux density (at 129 pc) relation for YSOs. The thick line gives the relation of Olofsson et al. (1999). The dotted line is the extrapolation to higher luminosities. The two filled diamonds correspond to the model calculations by Faison et al. (1998). The open circles connected by solid lines are our calculations using the DUSTY code (see text for details).

Table 6. Lower luminosity versus distance for YSOs detectable by ISOGAL at 7 μm

distance/kpc	0.129	1.0	5.0	10.0	20.0	25.0
Log(L/L$_\odot$)	-1.49	0.29	1.69	2.29	2.89	3.08

$$LogL/L_\odot = LogF_7/Jy + 0.34 \quad (6)$$

In order to extrapolate this relation to higher luminosities, we checked it against the predictions of the models described in Sect. 2.4. In Fig. 10 we reported as a dotted line the extrapolation of relation 6, the thick line corresponds to the range of fluxes and luminosities used by Olofsson et al. (1999). The open circles connected by solid lines are the DUSTY model results (scaled to the appropriate integrated flux at 129 pc) for central stars: G0, F5, F0, A5, A0, B5, B0, and O6. The three lines correspond to three different values of the overall optical depth of the envelope (τ_V=1, 10, and 100). The two filled diamonds represent two model results from Faison et al. (1998).

The fact that RCrA and Chamaleon star forming regions suffer little extinction makes the comparison between observed and model flux densities possible. Given our purpose of finding the approximate flux of a YSO for a given distance and luminosity, the agreement within 0.5 dex is adequate. In the following we shall assume that the logarithm of the 7 μm flux densities scale linearly with the logarithm of the luminosity according to Eq. 6 over the entire range of luminosities. In Table 6 we give the lower luminosity that a YSO must have in order to be detected at 7 μm as a function of its distance, obviously under the assumption of negligible line-of-sight extinction.

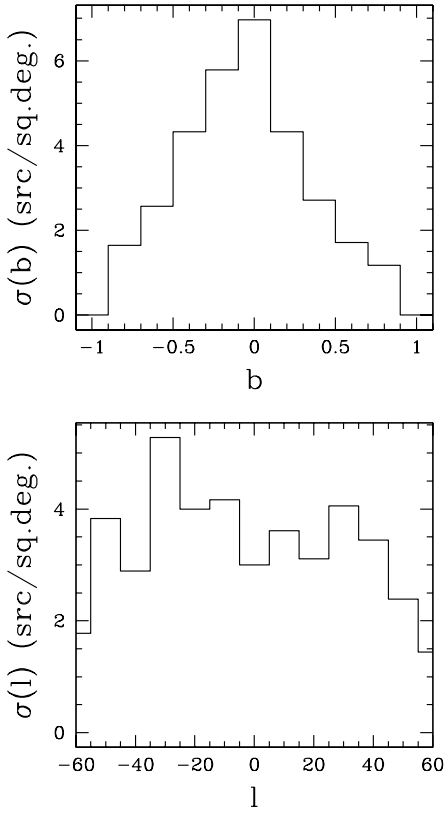

Fig. 11. Surface density of IRAS sources on the inner Galactic Plane, defined as $|l| < 70^\circ$ and $|b| < 0.9^\circ$, satisfying the WC89 colour criteria. Upper panel: surface density as a function of galactic latitude; lower panel: surface density as a function of galactic longitude.

From Table 6 we see that YSOs associated with early type stars with luminosities greater than $10^{2.5}$ L$_\odot$ should be detectable throughout the Galaxy (for Av = 0), while YSOs associated with stars of lower luminosities can be observed only up to increasingly smaller distances.

WC89 find that there are 1708 IRAS sources in the Galactic Plane that satisfy the colours criteria of UC HII regions. They also state that IRAS should detect at 12 μm all O9.5 ZAMS stars and hotter anywhere in the Galaxy. They estimate that their sample is dominated by the high-luminosity stars, with some nearby lower luminosity ones. To make the statement more quantitative, we shall use as a representative mean luminosity of the stars of the WC89 sample Log(L /L$_\odot$) = 4.5. In Fig. 11 we show the surface density distribution of IRAS sources satisfying the WC89 colour criteria in the inner Galactic Plane, defined as: $|l| < 70^\circ$ and $|b| < 0.9^\circ$. The latitude distribution clearly shows a strong concentration of sources toward the plane (see also WC89), while the longitude distribution is approximately flat for $l < |45^\circ|$, then falls in the outer Galaxy. We can see from Fig. 11 that for our fields at l=45° and $b < |0.9^\circ|$, we can assume an average surface density of $\sim$4 sources per square degree (see also TFT).

The increased sensitivity of ISOGAL with respect to IRAS will not increase the number of detected high luminosity stars, since both can detect them throughout the Galaxy. Considering

that the area covered by all the 5 ISOGAL fields is 0.504 square degrees (without overlap) and that we detect 3 high luminosity YSOs, the density is ∼6.0 sources per square degree, slightly higher than what derived from IRAS. Given the small numbers, this difference is probably not significant, nevertheless, we note that the IRAS PSC is highly incomplete on the Galactic plane (see also White et al. 1991), in fact only one of our 3 high luminosity YSOs is classified as an IRAS-WC89 source (the one coincident with TFT source 34).

The comparison between expected and observed densities of sources becomes more difficult for the lower luminosity YSOs. In this case we need to know the luminosity function of YSOs. Comerón & Torra (1996) give the following luminosity function for UCHII regions with luminosities greater than 10^4 $L_\odot$:

$$n(L)dL \propto L^{-1.9}dL \quad (7)$$

The integrated total number of sources will vary as $L^{-0.9}$. We do not know if the luminosity function can be extrapolated to lower luminosities. If it remains that steep, for luminosities two order of magnitude smaller than $10^{4.5}$ $L_\odot$, where ISOGAL is still able to detect a YSO throughout the Galaxy, we should have a surface density of approximately 250 sources per square degree. The total number of low luminosity YSOs and cYSOs is 108, which gives an observed density of ∼ 200 per square degree, slightly lower than but well within the expected range. However, the interstellar extinction at large distances may be not negligible and will reduce the number of sources above the detection limit. Moreover, YSOs are well known to be preferentially concentrated within dense molecular clouds, and the ISOGAL field at l=45° is in a region of low CO column density.

6. Conclusions

We used the 7 and 15 μm observations of five ISOGAL fields centered at l ∼ +45° and b ∼ 0°, obtained during the ISOGAL program, to search for low flux density YSOs which could not be detected with IRAS.

In order to separate the small number of YSOs from the much larger population of Post-MS stars we used primarily the position of the sources in the [15] - [7]-[15] diagram, which involves only ISOGAL data and allows to select objects with MIR excess as possible YSOs using the survey data alone. The criteria adopted are based on the results obtained in nearby star forming regions and galactic fields observed with ISOCAM, as well as theoretical indications.

The ISOGAL results were compared with radio observations in order to identify high luminosity YSOs out of the larger population of lower luminosity YSOs.

There are 386 point-like sources detected in both filters that satisfy the confidence conditions [7] < 9.5 and [15] < 8.

We found 3 high luminosity YSOs, 3 diffuse HII regions and 35 lower luminosity YSOs. The concentration is higher towards the Galactic Equator and regions of higher CO surface brightness.

We also found 73 sources detected only at 15 μm which, according to the colour upper limit, can be classified as candidate YSOs. However, the numerous weakest cYSOs needs to be validated since residual artefacts, such as false replication sources due to remanence effects, are possible.

The validity of the adopted criteria for selecting YSOs out of the ISOGAL observations are confirmed by four independent results: 1) the sources classified as YSOs and candidate YSOs are often associated with diffuse nebulosities visible at 15 μm and/or diffuse radio sources, which indicates abundance of diffuse gas and star forming activity, 2) all the bright YSOs have been found to be closely related to radio continuum emission, as expected, 3) one of the YSOs is associated with a water maser, and 4) the numbers of high luminosity and low luminosity YSOs that we found compare well with the expectations.

However, while the given list is a good starting point to search for low flux density YSOs in the Galactic Plane, it is clear that further broad band and spectroscopic observations are required to confirm present identifications.

Acknowledgements. We thank C. Alard and S. Ganesh for their contribution to data processing, and G. Simon for the preparation of the observations.

Appendix A: evaluation of errors of the ISOGAL observations in the C-D overlapping region

The LW2 and LW3 observations of fields C and D overlap in a ∼0.01 sq.deg. area and offer the possibility to compare the results of two independent sets of observations, as well as to evaluate the accuracy of the ISOGAL data. We will limit the discussion to the area common to the four observational datasets (C-7, C-15, D-7 and D-15). It is seen from Table 3 that it is a narrow strip, ∼0.26° long along the b axis and ∼0.06° wide along the l axis. Since the raster step along the l axis is 90″ (∼half-frame), there is a large fraction of this strip which is in the 90″ "edge strip" of one of the observations and has thus been observed half as long than regular ISOGAL observations: ∼80% at 15 μm and ∼40% at 7 μm. Most of the ISOGAL data from the inner part of the rasters is expected to have a much higher quality. In the total overlap area there are 72 sources in the C catalog (65 in C-7 and 26 in C-15) and 41 sources in the D catalog (35 in D-7 and 16 in D-15).

There are 36 sources in the overlapping part of C and D fields that can be associated within 6″ (corresponding to 1 pixel in the original ISOCAM images). The two datasets show a mean positional offset of $\leq 0.5''$ and a standard deviation of ∼1.5″, which shows that the astrometry is consistent in the two independent datasets.

Of the 36 common sources, 33 are common to the C-7 and D-7 datasets, 10 of these are also common to the C-15 and D-15 datasets (i.e. are detected in all four independent observations), 3 of the 33 are detected in the C-15 but not in the D-15 observations, all of these have $[15]_C \geq 8.2$. Of the 3 remaining sources 1 is detected at C-15 and D-7 (with $[7]_D$=10.2 and $[15]_C$=8.7) and two are detected at C-15 and D-15 but not in C-7 or D-7. We can see that the four common sources observed at C-15 but not at D-15 are fainter than 8.2, similarly the only common source detected at D-7 but not at C-7 is very faint.

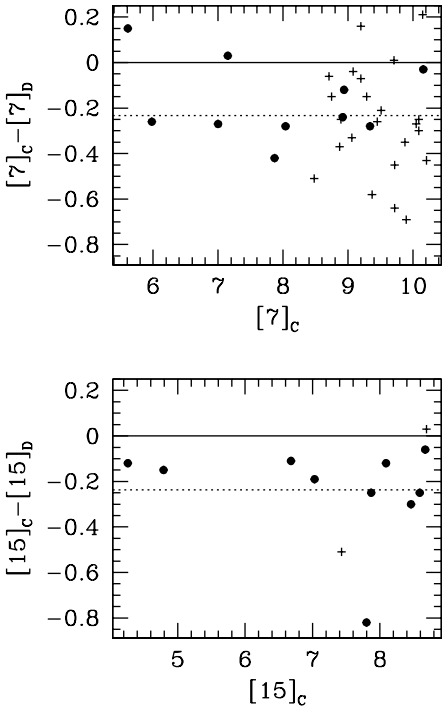

Fig. A.1. Difference between the observed magnitudes in the C-7 and D-7 observations (top panel) and the C-15 and D-15 (bottom panel) as a function of the C-7 and C-15 magnitudes, respectively. Sources detected in all four datasets are shown as filled circles. The dotted lines show the average difference.

In Fig. A.1, for the 33 sources common to the C-7 and D-7 and the 12 sources common to the C-15 and D-15 observations, we show the difference in the magnitudes measured in the C and D datasets as a function of the C magnitude. The 10 sources common to all four datasets are shown as filled circles. The dotted lines show the average magnitude difference, which is ∼–0.2 in both cases (the D magnitudes appear fainter at both [7] and [15]). The cause of this effect is still under investigation, it may be due to differences on the adopted point spread functions for the two fields. As expected the scatter in the magnitude difference gets larger for fainter sources.

In Fig. A.2 we show the magnitude distributions for sources in the common area of datasets C-7, C-15, D-7, and D-15. Shaded histograms correspond to sources common to the C and D datasets. The total numbers are 33 sources for C-7, 16 for C-15, 34 for D-7 and 12 for D-15. Open thick histograms are sources in the C-only or D-only datasets. The number of C-only sources is substantial, 36 in total (35 at C-7 and 10 at C-15), while only 1 out of the 35 D-7 sources and 4 of the 16 D-15 sources are not detected in the C datasets. As expected most of the C-only and D-only sources are at the faint end of the magnitudes distribution. The only exception is the D-15 source with $[15]_D$=6.75. This source is not detected at D-7 either and is most probably a ghost from a bright source not removed by the data reduction process because at the edge of the ISOGAL raster, in a region where there is no overlap between frames. Since we use the "vision" treatment procedure to reject such sources, only very few remain present in the catalog files, mainly near the edge of the images, where there is no overlap between several individual ISOCAM images. So they should not be statistically significant.

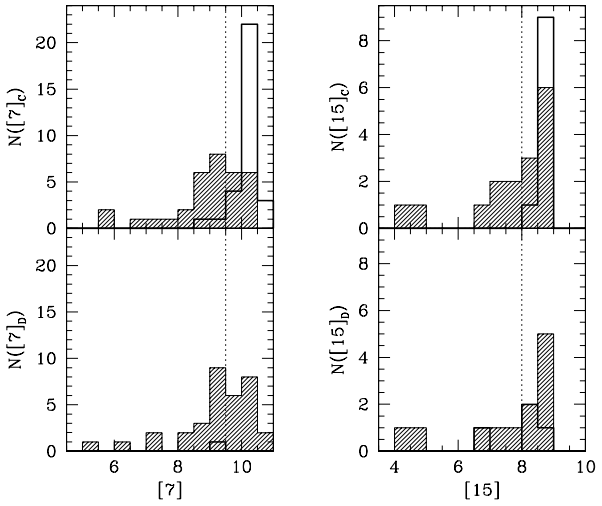

Fig. A.2. Magnitudes distributions for the four datasets C-7, C-15, D-7 and D-15 in the overlapping region. Top panels: C-7 (left) and C-15 (right); bottom panels: D-7 (left) and D-15 (right). Shaded histograms correspond to common sources in the C and D datasets (36 total), thick open histograms correspond to C-only (36 total) or D-only (5 total) sources. The vertical dotted lines represent the adopted confidence limits in the two bands.

With the exception of this source, we see that most of the sources detected only at C or only at D are fainter than [7]=9.5 and [15]=8.0.

We conclude from this comparison that, as in other fields, the confidence limits are [7] = 9.5 and [15] = 8. Thus, we only consider sources brighter than these limits in the discussion. We also conclude that the photometric errors, especially in the edge zones, can reach 0.5 magnitude even for sources one magnitude brighter than the confidence limit, and can be up to 0.8 magnitude for faint sources.

References

André P., Ward-Thompson D., Barsony M., 1993, ApJ 406, 122
Becker R.H., White R.L., Helfand D. J., Zoonematkermani S., 1994, ApJS 91, 347
Berrilli F., Corciulo G., Ingrosso G., et al., 1992, ApJ 398, 254
Blommaert J.A.D.L., 1998, ISOCAM Photometry Report, http://www.iso.vilspa.esa.es/users/expl_lib/CAM_list.html
Bontemps S., Nordh L., Olofsson G., et al., 1998, in: Yun J.L., Liseau r., (eds.), Star Formation with the Infrared Space Observatory, ASP Conference Series, Vol. 132, 1998, p. 141
Churchwell E., 1991, in: Lada C.J., Kylafis N.D. (eds.), The Physics of Star Formation and Early Stellar Evolution, Kluwer Academic Publishers, p. 221
Churchwell E., Wolfire M.G., Wood D.O.S., 1990, ApJ 354, 247
Comerón F., Torra J., 1996, A&A 314, 776
Condon J.J., Cotton W.D., Greisen E.W., et al., 1998, ApJ 115, 1693
Dame T.M., Ungerechts H., Cohen R.S., et al., 1987, ApJ 322, 706
Faison M., Churchwell E., Hofner P., et al., 1998, ApJ, 500, 280

Felli M., Cesaroni R., Palla F., Testi L., 2000, in preparation
Glass I.S., Ganesh S., Alard C., et al., 1999, MNRAS 308, 127
Hillenbrand L.A., Strom S.E., Vrba F.J., Keene J., 1992, ApJ 397, 613
1995, A&A 302, 249
Ivezić Z., Elitzur M., 1997, MNRAS 287, 799
Jiang B.W., Omont A., Ganesh S., Simon G., 2000, in preparation
Lada C.J., 1999, The Origin of Stars and Planetary System, C.J. Lada and N.D. Kylafis, eds, Dordrecht: Kluwer Academic Press, in press
Lada C.J., Wilking B.A., 1984, ApJ 287, 610
Miroshnichenko A., Ivezsić Z., Elitzur M., 1997, ApJ 475, L41
Miroshnichenko A., Ivezsić Z., Vinkovic D., Elitzur M., 1999, ApJ 520, L115
Molinari S., Testi L., Brand J., Cesaroni R., Palla F., 1998, ApJ 505, L39
Natta A., 1999, in: Casoli F., David F., Lequeux J. (eds.), Infrared space astronomy, to-day and to-morrow, EDP-Sciences, Springer-Verlag
Nordh L., Olofsson G., Bontemps S., et al., 1998, in: Yun J.L., Liseau R. (eds.), Star Formation with the Infrared Space Observatory, ASP Conference Series, Vol. 132, 1998, p. 127
Olofsson G., Abergel A., Andrè Ph., et al., 1996, A&A 315, L185
Olofsson G., Huldtgren M., Kaas A.A., et al., 1999, A&A 350, 883
Omont A., Ganesh S., Alard C., et al., 1999a, A&A 348, 755
Omont A., & The ISOGAL Collaboration, 1999b, in: Bicay M.C., Beichman C.A., Cutri R.M., Madore B.F. (eds.), Astrophysics with Infrared Surveys: A Prelude to SIRTF, ASP Conference Series Vol. 177.
Omont A., & The Isogal Collaboration, 2000, Springer Lecture Notes of Physics Series, as part of the proceedings for "ISO Surveys of a Dusty Universe," a workshop held at Ringberg Castle, Germany, November 8–12, 1999
Ortiz R., Blommaert J.A.D.L., Copet E., et al., 2000, submitted to A&A
Pérault M., Omont A., Simon G., et al., 1996, A&A 315, L165
Pezzuto S., Strafella F., Lorenzetti D., 1997, ApJ 485, 290
Reid M.J., Argon L., Masson C.R., Menten K.M., Moran J.M., 1995, ApJ 443, 238
Rowan-Robinson M., 1980, ApJS 44, 403
Schmidt-Kaler Th., 1981, in Landolt-Börnstein, Gruppe IV, Band 2, 1. Publ. Springer
Schuller F., et al., 2000, in preparation
Scoville N.Z., Kwan J., 1976, ApJ 206, 718
Testi L., Felli M., Pérault M., et al., 1997, A&A 318, L13.
Testi L., Felli M., Taylor G.B., 1999, A&AS 138, 71
White R.L., Becker R.H., Helfand, D.J., 1991, ApJ 371, 148
Wood D.O.S., Churchwell E., 1989, ApJ 340, 265